JOURNAL OF MATERIALS PROCESSING TECHNOLOGY 205 (2008) 514–515

ELSEVIER

available at www.sciencedirect.com

ScienceDirect

journal homepage: www.elsevier.com/locate/jmatprotec

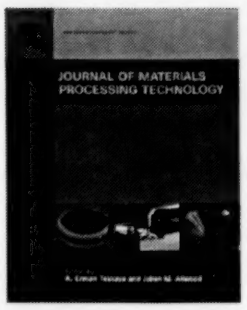

Author Index of Volume 205

Abrinia, K., 259
Aggarwal, A., 42
Ahrens, S., 111
Alain, M., 322
Altan, T., 459
Asfour, S., 190
Azizi Mohd Azizli, K., 119

Babaei, R., 506
Barbosa, C.A., 353
Bayramoglu, M., 394
Bhattacharyya, B., 376
Bi, J., 9
Bin, S., 207
Boopathy, S.R., 235
Boudeau, N., 51
Bressan, J.D., 353
Buranathiti, T., 451
Byon, S.M., 70

Cai, C., 214
Cao, X., 322
Çetin, A., 1
Cha, H.-M., 160
Chakraborty, P., 190
Chen, B., 316
Chen, C., 432
Chen, D., 432
Chen, M.-S., 308
Chen, Y., 9
Cho, S., 190
Cui, Y., 138
Cui, Z., 497

Dadashzadeh, M., 506
Daros, D.P., 353
Davami, P., 506
Davim, J.P., 16
Denti, L., 489
Dinhut, J.F., 151
Dong, Q.-m., 366

E, D., 469
Eivani, A.R., 388
Emanian, E., 283

Fan, J.H., 316
Fang, C.-C., 128
Folle, L.F., 347
Fournier, J., 322
Fu, K.-J., 243
Fu, P., 224
Fuad Saiyid Hashim, S., 119

Gaitonde, V.N., 16
Ganesan, P., 272
Gao, H., 214
Gatto, A., 489
Geng, H., 146
Geren, N., 394
Gindy, N., 338
Goodwin, F.E., 459
Grosseau-Poussard, J.L., 151
Guo, L., 99

Haseeb, A.S.M.A., 203
Hatami, N., 506
Hojjati, M.H., 482
Hosseinipour, S.J., 482
Hsu, C.-C., 249
Hussin, H., 119
Huvier, C., 151

Im, Y.T., 70
Iuliano, L., 489

Jahazi, M., 322
Jeong, H., 360
Jiang, H., 224
Jiang, Y., 303
Jiang, Z., 303
Jiao, X., 432
Jung, Y.-G., 160

Kahraman, R., 183
Kalkanli, A., 1
Kang, J.-H., 160
Karimi, D., 283
Karnik, S.R., 16
Kim, H., 459
Kim, H.Y., 70
Kokabi, A.H., 60
Kolenbrander, M., 297
Kositpipat, A., 451
Kulczyk, M., 173
Kumar, P., 42
Kurzydlowski, K.J., 173
Kwon, H.C., 70

Lee, H.W., 70
Lei, L., 207
Leonelli, C., 489
Li, B., 370
Li, C., 497
Li, H.-j., 366
Li, L., 99
Li, S., 34
Li, Y., 146
Li, Z., 469
Li, Z.-R., 243
Liao, Y.-S., 24
Lin, G., 419
Lin, Y.C., 308
Liu, F., 243
Liu, J., 497
Liu, N., 411
Liu, P., 146, 366
Lu, C., 439
Lu, J., 9
Lu, M., 411
Luo, A.A., 224
Lynn, M., 190

Makaremi, M., 259
Mazur, A., 173
Mesquita, R.A., 353
Milhet, X., 151
Mitra, S., 376
Mizuno, T., 469
Mohammadi, A., 283
Mücklich, S., 111

Naher, S., 203
Nash, P., 477
Ni, X., 9
Nigrelli, V., 290
Nodeh, I.R., 60

Onar, A., 190
Ozdemir, I., 111

Pachla, W., 173
Paik, U., 160
Palaniandy, S., 119
Park, B., 360
Park, H.D., 70
Park, J., 360
Park, K., 360
Pasta, S., 290
Peng, L., 224
Peng, X.H., 316
Pengpat, K., 168
Polat, H., 394

Elsevier B.V.
doi:10.1016/S0924-0136(08)00470-6

Poshal, G., 272
Prapitpongwanich, P., 168

Ramesh, A., 235
Rash Ahmadi, S., 89
Ren, F.-z., 366

Sachdev, A.K., 224
Sadough, A., 89
Sarkar, S., 376
Schaeffer, L., 347
Sekh, M., 376
Senthilkumaran, S., 235
Serajzadeh, S., 60
Shakeri, M., 89
Shen, D.-J., 477
Sheng, Z.Q., 81
Shiou, F.-J., 249
Silveira Netto, S.E., 347
Singh, H., 42
Singh, M., 42
Singjai, P., 168
Sokolowski, A., 353
Song, X., 138
Su, J.-h., 366
Suganth kumar, K.J., 235
Sun, S.T., 316
Sun, Z., 99
Sunar, M., 183
Sung, J., 459
Sus-Ryszkowska, M., 173

Taheri, A.K., 388
Tang, X., 404
Tehrani, A.F., 283
Tian, C., 411
Ting, D., 425
Tsai, C.-L., 24

Vaezi, M.R., 332
Velasco, R., 51
Veronesi, P., 489

Wang, F., 303
Wang, J., 146
Wang, L.-J., 243
Wang, Y., 338
Wang, Y.-L., 477
Wang, Z., 34, 338
Wei, Y., 432
Wenbin, H., 207
Wielage, B., 111
Wu, L., 214
Wu, Y., 34
Wu, Z., 303
Xie, J., 338
Xing, G.-Z., 477
Xu, P., 404
Xu, Z., 419

Yan, M.-T., 128
Yang, H., 99
Yao, S., 404
Yao, Z., 303
Yating, W., 207
Yilbas, B., 183
Yu, Y., 224
Yuqi, L., 425

Zaspalis, V.T., 297
Zhai, C., 224
Zhang, G., 214
Zhang, G.L., 370
Zhang, H., 214
Zhang, H.Q., 370
Zhang, S.H., 370
Zhang, X., 9
Zhang, Z.X., 419
Zhibing, Z., 425
Zhigang, L., 425
Zhong, J., 308
Zoorabadi, M., 482

JOURNAL OF MATERIALS PROCESSING TECHNOLOGY 205 (2008) 516–523

available at www.sciencedirect.com

ScienceDirect

journal homepage: www.elsevier.com/locate/jmatprotec

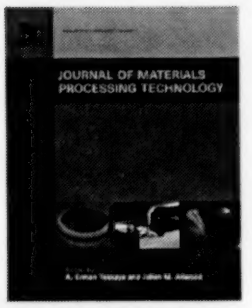

Subject Index of Volume 205

Abaqus
A parametric FEA system for fixturing of thin-walled cylindrical components, 338
Acid leaching
Production and purification of zircon opacifier from zircon found in the coastal area of Bangladesh, 203
Adhesive
Influence of adhesive thickness and filler content on the mechanical performance of aluminum single-lap joints bonded with aluminum powder filled epoxy adhesive, 183
ADSAW
Fundamental studies on in-process controlling angular distortion in asymmetrical double-sided double arc welding, 214
Advanced high strength steel (AHSS)
Investigation of galling in forming galvanized advanced high strength steels (AHSSs) using the twist compression test (TCT), 459
Aging kinetics
Modeling age hardening kinetics of an Al–Mg–Si–Cu aluminum alloy, 388
AISI P-20 tool steel
Optimization of multiple quality characteristics for CNC turning under cryogenic cutting environment using desirability function, 42
Al–Mg–Si–Cu aluminum alloy
Modeling age hardening kinetics of an Al–Mg–Si–Cu aluminum alloy, 388
Al_2O_3 reinforcement
Nanocrystalline Al–Al_2O_{3p} and SiC_p composites produced by high-energy ball milling, 111
Aluminium 5083
Optimization of superplastic hydroforming process of Aluminium alloy 5083, 482
Aluminum
Influence of adhesive thickness and filler content on the mechanical performance of aluminum single-lap joints bonded with aluminum powder filled epoxy adhesive, 183
Aluminum alloy
Analysis of the manufacturing process of beverage cans using aluminum alloy, 347
Aluminum matrix composites
Nanocrystalline Al–Al_2O_{3p} and SiC_p composites produced by high-energy ball milling, 111
AM50
Low-pressure die casting of magnesium alloy AM50: Response to process parameters, 224
Analytical modeling
Tube bulging test: Theoretical analysis and numerical validation, 51
Angular distortion
Fundamental studies on in-process controlling angular distortion in asymmetrical double-sided double arc welding, 214
Arc distance
Fundamental studies on in-process controlling angular distortion in asymmetrical double-sided double arc welding, 214
Artificial neural network
Investigations into the effect of cutting conditions on surface roughness in turning of free machining steel by ANN models, 16

Ball burnishing process
Surface finishing of hardened and tempered stainless tool steel using sequential ball grinding, ball burnishing and ball polishing processes on a machining centre, 249
Ball-end milling
Prediction of cutting forces in ball-end milling by means of geometric analysis, 24
$BaTiO_3$
Crack suppression and residual stress in $BaTiO_3$ based Ni-MLCCs of Y5V specification through post-process, 160
Beverage cans
Analysis of the manufacturing process of beverage cans using aluminum alloy, 347
Blank design
Blank design and formability prediction of complicated progressive die stamping part using a multi-step unfolding method, 425
Blank holding force
Stress analysis of rectangular cup drawing, 469
Body jack case
Analysis and design of body jack case stamping for fewer production steps, 451
Break-in delay
Correlation between break-in characteristics and pad surface conditions in silicon wafer polishing, 360
Break-in time
Correlation between break-in characteristics and pad surface conditions in silicon wafer polishing, 360
Buffing process
Correlation between break-in characteristics and pad surface conditions in silicon wafer polishing, 360

Elsevier B.V.
doi:10.1016/S0924-0136(08)00471-8

Ceramic coatings
Preparation and structure of ceramic coatings containing zirconium oxide on Ti alloy by plasma electrolytic oxidation, 303
Ceramic matrix composites
Synthesis of silicon carbide/aluminium tetroxycarbide nanofibres for reinforcement of glass matrix composites: Material properties, 168
Ceramics
Mixing homogeneity and its influence on the manufacturing process and properties of soft magnetic ceramics, 297
Circle cutting
Applying parallelogrammic strips for cutting circles from stainless steel rolls, 138
Circular laser
Application of circular laser vision sensor (CLVS) on welded seam tracking, 404
Clustering
Effect of solidification rate on spatial distribution of SiC particles in A356 alloy composites, 1
CNC turning
Optimization of multiple quality characteristics for CNC turning under cryogenic cutting environment using desirability function, 42
Coating
Stress analysis in thin coatings and substrate subjected to point contact loading (mechanics of scratch test), 89
Cost and performance evaluation of different surface treated dies for hot forging process, 394
Coatings
Consolidation of iron powders through the influence of phosphate thin films, 151
Cold-expansion of holes
Finite-element simulation of residual stress induced by split-sleeve cold-expansion process of holes, 290
Composites
Effect of solidification rate on spatial distribution of SiC particles in A356 alloy composites, 1
Constitutive equation
Effect of temperature and strain rate on the compressive deformation behavior of 42CrMo steel, 308
A viscous-elastoplastic constitutive equation incorporating phase transformation with the application to the residual stress analysis for welding process, 316
Converging and diverging surfaces
A new three-dimensional solution for the extrusions of sections with larger dimensions than the initial billet, 259
Copper surface segregation
Effects of light pre-deformation on pitting corrosion resistance of copper-bearing ferrite antibacterial stainless steel, 419
Corrosion resistance
Preparation and structure of ceramic coatings containing zirconium oxide on Ti alloy by plasma electrolytic oxidation, 303
Crack suppression
Crack suppression and residual stress in $BaTiO_3$ based Ni-MLCCs of Y5V specification through post-process, 160

42CrMo steel
Effect of temperature and strain rate on the compressive deformation behavior of 42CrMo steel, 308
Crosslinking reaction
Synthesis of a novel perfluorinated acrylate copolymer containing hydroxyethyl sulfone as crosslinking group and its application on cotton fabrics, 243
Cryogenic cutting environment
Optimization of multiple quality characteristics for CNC turning under cryogenic cutting environment using desirability function, 42
Crystallite size
Nanocrystalline Al–Al_2O_{3p} and SiC_p composites produced by high-energy ball milling, 111
Cu–Cr–Sn–Zn alloy
Aging study of rapidly solidified and solid-solution Cu–Cr–Sn–Zn alloy, 366
Cutting force
Prediction of cutting forces in ball-end milling by means of geometric analysis, 24
Cutting stock
Applying parallelogrammic strips for cutting circles from stainless steel rolls, 138
Cylindrical components
A parametric FEA system for fixturing of thin-walled cylindrical components, 338

3D
Application of circular laser vision sensor (CLVS) on welded seam tracking, 404
DC casting
Modeling of hot tearing formation during solidification, 506
Design
Statistical analysis of wire electrical discharge turning on material removal rate, 283
Desirability function
Optimization of multiple quality characteristics for CNC turning under cryogenic cutting environment using desirability function, 42
Modeling and optimization of wire electrical discharge machining of γ-TiAl in trim cutting operation, 376
Die cost
Cost and performance evaluation of different surface treated dies for hot forging process, 394
Die life
Cost and performance evaluation of different surface treated dies for hot forging process, 394
Diffusion
Microstructure and XRD analysis in the interface zone of Mg/Al diffusion bonding, 146
Distortion controlling
Fundamental studies on in-process controlling angular distortion in asymmetrical double-sided double arc welding, 214
DRX
Analysis of metal workability by integration of FEM and 3-D processing maps, 497
Dry machining
Modeling tool wear progression by using mixed effects modeling technique when end-milling AISI 4340 steel, 190

EDX analysis
Modeling tool wear progression by using mixed effects modeling technique when end-milling AISI 4340 steel, 190
Electroless nickel plating
Artificial neural network modelling of plating rate and phosphorus content in the coatings of electroless nickel plating, 207

End-milling
Modeling tool wear progression by using mixed effects modeling technique when end-milling AISI 4340 steel, 190
Epoxy
Influence of adhesive thickness and filler content on the mechanical performance of aluminum single-lap joints bonded with aluminum powder filled epoxy adhesive, 183
Epsilon copper precipitation
Effects of light pre-deformation on pitting corrosion resistance of copper-bearing ferrite antibacterial stainless steel, 419
Error evaluation
Tube bulging test: Theoretical analysis and numerical validation, 51
Extrusion
A new three-dimensional solution for the extrusions of sections with larger dimensions than the initial billet, 259

Face centered central composite design
Optimization of multiple quality characteristics for CNC turning under cryogenic cutting environment using desirability function, 42
Fastener holes
Finite-element simulation of residual stress induced by split-sleeve cold-expansion process of holes, 290
FE simulations
Tube bulging test: Theoretical analysis and numerical validation, 51
FEA
A parametric FEA system for fixturing of thin-walled cylindrical components, 338
FEM
Stress analysis in thin coatings and substrate subjected to point contact loading (mechanics of scratch test), 89
Analysis of metal workability by integration of FEM and 3-D processing maps, 497
FEM analysis
A new three-dimensional solution for the extrusions of sections with larger dimensions than the initial billet, 259
Ferrite antibacterial stainless steel
Effects of light pre-deformation on pitting corrosion resistance of copper-bearing ferrite antibacterial stainless steel, 419
Ferrites
Mixing homogeneity and its influence on the manufacturing process and properties of soft magnetic ceramics, 297
Finite element analysis
Simulation of welding residual stresses in resistance spot welding, FE modeling and X-ray verification, 60
A viscous-elastoplastic constitutive equation incorporating phase transformation with the application to the residual stress analysis for welding process, 316
Investigation of galling in forming galvanized advanced high strength steels (AHSSs) using the twist compression test (TCT), 459
Finite element modeling
Optimization of superplastic hydroforming process of Aluminium alloy 5083, 482
Finite-element simulation
Finite-element simulation of residual stress induced by split-sleeve cold-expansion process of holes, 290
Flow instability
Analysis of metal workability by integration of FEM and 3-D processing maps, 497
Flow stress
Effect of temperature and strain rate on the compressive deformation behavior of 42CrMo steel, 308
Forging
Cost and performance evaluation of different surface treated dies for hot forging process, 394
Formability
Formability of tailor-welded strips and progressive forming test, 81
Analysis and design of body jack case stamping for fewer production steps, 451
Forming limit curve
Analysis of the manufacturing process of beverage cans using aluminum alloy, 347
Free form
Statistical analysis of wire electrical discharge turning on material removal rate, 283
Free machining steel
Investigations into the effect of cutting conditions on surface roughness in turning of free machining steel by ANN models, 16
Friction coefficient
Analysis of the manufacturing process of beverage cans using aluminum alloy, 347
Fuzzy logic controller
Application of genetic algorithm-based fuzzy logic control in wire transport system of wire-EDM machine, 128

Galling
Investigation of galling in forming galvanized advanced high strength steels (AHSSs) using the twist compression test (TCT), 459
Genetic algorithm
Application of genetic algorithm-based fuzzy logic control in wire transport system of wire-EDM machine, 128
Grain refinement
Nanocrystalline titanium produced by hydrostatic extrusion, 173
Grinding
Relationship between subsurface damage and surface roughness of optical materials in grinding and lapping processes, 34
Guide roll
A control method of guide rolls in 3D-FE simulation of ring rolling, 99

Heat treatment
Consolidation of iron powders through the influence of phosphate thin films, 151
Influence of hardness on the wear resistance of 17-4 PH stainless steel evaluated by the pin-on-disc testing, 353
High-energy ball milling
Nanocrystalline Al–Al_2O_{3p} and SiC_p composites produced by high-energy ball milling, 111
Hot bar rolling
Processing map approach for surface defect prediction in the hot bar rolling, 70
Hot compression deformation
Effect of temperature and strain rate on the compressive deformation behavior of 42CrMo steel, 308

Hot compression tests
Processing map approach for surface defect prediction in the hot bar rolling, 70
Hot tear criterion
Modeling of hot tearing formation during solidification, 506
Hydraulic adjustment mechanism
A control method of guide rolls in 3D-FE simulation of ring rolling, 99
Hydrostatic extrusion
Nanocrystalline titanium produced by hydrostatic extrusion, 173

Instability
Processing map approach for surface defect prediction in the hot bar rolling, 70
Intermetallic compounds
Microstructure and XRD analysis in the interface zone of Mg/Al diffusion bonding, 146
Inverse approach
Blank design and formability prediction of complicated progressive die stamping part using a multi-step unfolding method, 425
Ironing
Analysis of the manufacturing process of beverage cans using aluminum alloy, 347

Jet mill
Mechanochemistry of silica on jet milling, 119
Joining mechanism
Microwave assisted sintering of green metal parts, 489
Joints
Influence of adhesive thickness and filler content on the mechanical performance of aluminum single-lap joints bonded with aluminum powder filled epoxy adhesive, 183

Lapping
Relationship between subsurface damage and surface roughness of optical materials in grinding and lapping processes, 34
Large deformation
Optimization of superplastic hydroforming process of Aluminium alloy 5083, 482
Laser heating
Plastic penetration during laser heating of a metal plate, 9
Laser surface cladding
Optimization of bead spacing during laser cladding of ZE41A-T5 magnesium alloy castings, 322
Lattice strain
Nanocrystalline Al–Al_2O_{3p} and SiC_p composites produced by high-energy ball milling, 111
Layer distance
Optimization of bead spacing during laser cladding of ZE41A-T5 magnesium alloy castings, 322
Light pre-deformation
Effects of light pre-deformation on pitting corrosion resistance of copper-bearing ferrite antibacterial stainless steel, 419
Low temperature
$SrTi_{1-x}Zr_xO_3$ uniform particles: Low-temperature synthesis, characterization and sintered properties, 432
Low-pressure die casting
Low-pressure die casting of magnesium alloy AM50: Response to process parameters, 224

Machining
Study on prediction of surface quality in machining process, 439
Magnesium alloy
Low-pressure die casting of magnesium alloy AM50: Response to process parameters, 224
Optimization of bead spacing during laser cladding of ZE41A-T5 magnesium alloy castings, 322
Magnetic molding
Theoretical and experimental investigation of mold strength in magnetic molding compacts, 235
Material characterization
Tube bulging test: Theoretical analysis and numerical validation, 51
Material flow
A new three-dimensional solution for the extrusions of sections with larger dimensions than the initial billet, 259
Material removal rate
Statistical analysis of wire electrical discharge turning on material removal rate, 283
Mechanical properties
Consolidation of iron powders through the influence of phosphate thin films, 151
Synthesis of silicon carbide/aluminium tetroxycarbide nanofibres for reinforcement of glass matrix composites: Material properties, 168
Effect of WC on microstructure and mechanical properties of silicon nitride nano-composites, 411
Mechanochemical effect
Mechanochemistry of silica on jet milling, 119
Metal filler
Influence of adhesive thickness and filler content on the mechanical performance of aluminum single-lap joints bonded with aluminum powder filled epoxy adhesive, 183
Microstructures
Microstructure and XRD analysis in the interface zone of Mg/Al diffusion bonding, 146
Aging study of rapidly solidified and solid-solution Cu–Cr–Sn–Zn alloy, 366
Effect of WC on microstructure and mechanical properties of silicon nitride nano-composites, 411
Microstructure, temperature estimation and thermal shock resistance of PEO ceramic coatings on aluminum, 477
Microwave sintering
Microwave assisted sintering of green metal parts, 489
Micro-Wire-EDM
Application of genetic algorithm-based fuzzy logic control in wire transport system of wire-EDM machine, 128
Minimum energy method
Prediction of cutting forces in ball-end milling by means of geometric analysis, 24
Mixed effects model
Modeling tool wear progression by using mixed effects modeling technique when end-milling AISI 4340 steel, 190
Mixing homogeneity
Mixing homogeneity and its influence on the manufacturing process and properties of soft magnetic ceramics, 297
Modeling
Modeling age hardening kinetics of an Al–Mg–Si–Cu aluminum alloy, 388
Modeling of hot tearing formation during solidification, 506

Modelling
Artificial neural network modelling of plating rate and phosphorus content in the coatings of electroless nickel plating, 207
Mold strength
Theoretical and experimental investigation of mold strength in magnetic molding compacts, 235
MRF
Relationship between subsurface damage and surface roughness of optical materials in grinding and lapping processes, 34
Multilayer ceramic capacitors (MLCCs)
Crack suppression and residual stress in $BaTiO_3$ based Ni-MLCCs of Y5V specification through post-process, 160
Multimode applicator
Microwave assisted sintering of green metal parts, 489
Multi-response optimization
Optimization of multiple quality characteristics for CNC turning under cryogenic cutting environment using desirability function, 42
Multi-step unfolding method
Blank design and formability prediction of complicated progressive die stamping part using a multi-step unfolding method, 425

Nano-composite materials
Two-step solochemical synthesis of ZnO/TiO_2 nano-composite materials, 332
Nano-composites
Synthesis of silicon carbide/aluminium tetroxycarbide nanofibres for reinforcement of glass matrix composites: Material properties, 168
Effect of WC on microstructure and mechanical properties of silicon nitride nano-composites, 411
Nanocrystalline
Nanocrystalline titanium produced by hydrostatic extrusion, 173
Nanofibres
Synthesis of silicon carbide/aluminium tetroxycarbide nanofibres for reinforcement of glass matrix composites: Material properties, 168
Nd:YAG laser
Optimization of bead spacing during laser cladding of ZE41A-T5 magnesium alloy castings, 322
Neural network
Artificial neural network modelling of plating rate and phosphorus content in the coatings of electroless nickel plating, 207
An analysis of formability of aluminium preforms using neural network, 272
Nonlinear finite element analysis
Analysis and design of body jack case stamping for fewer production steps, 451
Numerical simulation
Fundamental studies on in-process controlling angular distortion in asymmetrical double-sided double arc welding, 214

Opacifier
Production and purification of zircon opacifier from zircon found in the coastal area of Bangladesh, 203
Optical materials
Relationship between subsurface damage and surface roughness of optical materials in grinding and lapping processes, 34
Optimal spherical polishing parameters
Surface finishing of hardened and tempered stainless tool steel using sequential ball grinding, ball burnishing and ball polishing processes on a machining centre, 249
Orthogonal array
Investigations into the effect of cutting conditions on surface roughness in turning of free machining steel by ANN models, 16
Orthogonal experiment
Artificial neural network modelling of plating rate and phosphorus content in the coatings of electroless nickel plating, 207

Pad
Correlation between break-in characteristics and pad surface conditions in silicon wafer polishing, 360
Parametric
A parametric FEA system for fixturing of thin-walled cylindrical components, 338
Pareto optimization
Modeling and optimization of wire electrical discharge machining of γ-TiAl in trim cutting operation, 376
Perfluorinated acrylate copolymer
Synthesis of a novel perfluorinated acrylate copolymer containing hydroxyethyl sulfone as crosslinking group and its application on cotton fabrics, 243
PH stainless steel
Influence of hardness on the wear resistance of 17-4 PH stainless steel evaluated by the pin-on-disc testing, 353
Phase transformation
A viscous-elastoplastic constitutive equation incorporating phase transformation with the application to the residual stress analysis for welding process, 316
Phosphorus
Consolidation of iron powders through the influence of phosphate thin films, 151
Pitting corrosion resistance
Effects of light pre-deformation on pitting corrosion resistance of copper-bearing ferrite antibacterial stainless steel, 419
Plasma electrolytic oxidation
Preparation and structure of ceramic coatings containing zirconium oxide on Ti alloy by plasma electrolytic oxidation, 303
Microstructure, temperature estimation and thermal shock resistance of PEO ceramic coatings on aluminum, 477
Plastic deformation heat
Prediction of 3-D temperature field of TP2 copper tubes in three-roll planetary rolling process, 370
Post-process
Crack suppression and residual stress in $BaTiO_3$ based Ni-MLCCs of Y5V specification through post-process, 160
Powder preforms
An analysis of formability of aluminium preforms using neural network, 272
Power dissipation efficiency
Analysis of metal workability by integration of FEM and 3-D processing maps, 497
Process optimization
Optimization of bead spacing during laser cladding of ZE41A-T5 magnesium alloy castings, 322

Process parameter
Low-pressure die casting of magnesium alloy AM50: Response to process parameters, 224
Processing maps
Processing map approach for surface defect prediction in the hot bar rolling, 70
Analysis of metal workability by integration of FEM and 3-D processing maps, 497
Processing parameters
Effect of temperature and strain rate on the compressive deformation behavior of 42CrMo steel, 308
Progressive die
Blank design and formability prediction of complicated progressive die stamping part using a multi-step unfolding method, 425
Progressive forming
Formability of tailor-welded strips and progressive forming test, 81
Properties
Aging study of rapidly solidified and solid-solution Cu–Cr–Sn–Zn alloy, 366

Radial stress
Stress analysis of rectangular cup drawing, 469
Rapidly solidified aging
Aging study of rapidly solidified and solid-solution Cu–Cr–Sn–Zn alloy, 366
Rectangular cup drawing
Stress analysis of rectangular cup drawing, 469
Residual stress
Simulation of welding residual stresses in resistance spot welding, FE modeling and X-ray verification, 60
Crack suppression and residual stress in $BaTiO_3$ based Ni-MLCCs of Y5V specification through post-process, 160
Finite-element simulation of residual stress induced by split-sleeve cold-expansion process of holes, 290
Resistance spot welding
Simulation of welding residual stresses in resistance spot welding, FE modeling and X-ray verification, 60
Ring rolling
A control method of guide rolls in 3D-FE simulation of ring rolling, 99
Roughing mill
Processing map approach for surface defect prediction in the hot bar rolling, 70
RSM
Modeling and optimization of wire electrical discharge machining of γ-TiAl in trim cutting operation, 376

Scratch test
Stress analysis in thin coatings and substrate subjected to point contact loading (mechanics of scratch test), 89
Seam tracking
Application of circular laser vision sensor (CLVS) on welded seam tracking, 404
Semi-dry machining
Modeling tool wear progression by using mixed effects modeling technique when end-milling AISI 4340 steel, 190
Severe plastic deformation
Nanocrystalline titanium produced by hydrostatic extrusion, 173
Shaped sections
A new three-dimensional solution for the extrusions of sections with larger dimensions than the initial billet, 259
Sheet metal stamping
Analysis and design of body jack case stamping for fewer production steps, 451
SiC reinforcement
Nanocrystalline Al–Al_2O_{3p} and SiC_p composites produced by high-energy ball milling, 111
Silica
Mechanochemistry of silica on jet milling, 119
Silicon nitride
Effect of WC on microstructure and mechanical properties of silicon nitride nano-composites, 411
Sintered aluminium
An analysis of formability of aluminium preforms using neural network, 272
Sintering properties
$SrTi_{1-x}Zr_xO_3$ uniform particles: Low-temperature synthesis, characterization and sintered properties, 432
Solidification
Effect of solidification rate on spatial distribution of SiC particles in A356 alloy composites, 1
Solid-solution aging
Aging study of rapidly solidified and solid-solution Cu–Cr–Sn–Zn alloy, 366
Solochemical processing
Two-step solochemical synthesis of ZnO/TiO_2 nano-composite materials, 332
Spherical polishing process
Surface finishing of hardened and tempered stainless tool steel using sequential ball grinding, ball burnishing and ball polishing processes on a machining centre, 249
Spread extrusion
A new three-dimensional solution for the extrusions of sections with larger dimensions than the initial billet, 259
$SrTi_{1-x}Zr_xO_3$
$SrTi_{1-x}Zr_xO_3$ uniform particles: Low-temperature synthesis, characterization and sintered properties, 432
Stainless steel rolls
Applying parallelogrammic strips for cutting circles from stainless steel rolls, 138
Stamping
Investigation of galling in forming galvanized advanced high strength steels (AHSSs) using the twist compression test (TCT), 459
Statistical analysis
Statistical analysis of wire electrical discharge turning on material removal rate, 283
Steel shots sizes
Theoretical and experimental investigation of mold strength in magnetic molding compacts, 235
Stir-casting
Effect of solidification rate on spatial distribution of SiC particles in A356 alloy composites, 1
Straight/curve flange
Stress analysis of rectangular cup drawing, 469
Strain-hardening exponent
Analysis of the manufacturing process of beverage cans using aluminum alloy, 347
Stress analysis
Stress analysis in thin coatings and substrate subjected to point contact loading (mechanics of scratch test), 89
Subsurface damage
Relationship between subsurface damage and surface roughness of optical materials in grinding and lapping processes, 34

Superplastic forming
Optimization of superplastic hydroforming process of Aluminium alloy 5083, 482
Surface profile prediction
Study on prediction of surface quality in machining process, 439
Surface roughness
Investigations into the effect of cutting conditions on surface roughness in turning of free machining steel by ANN models, 16
Relationship between subsurface damage and surface roughness of optical materials in grinding and lapping processes, 34
Correlation between break-in characteristics and pad surface conditions in silicon wafer polishing, 360
Surface roughness prediction
Study on prediction of surface quality in machining process, 439

Taguchi's method
Surface finishing of hardened and tempered stainless tool steel using sequential ball grinding, ball burnishing and ball polishing processes on a machining centre, 249
Tailor-welded strip
Formability of tailor-welded strips and progressive forming test, 81
Temperature calculation formula
Microstructure, temperature estimation and thermal shock resistance of PEO ceramic coatings on aluminum, 477
Temperature field
Plastic penetration during laser heating of a metal plate, 9
Prediction of 3-D temperature field of TP2 copper tubes in three-roll planetary rolling process, 370
Thermal shock
Microstructure, temperature estimation and thermal shock resistance of PEO ceramic coatings on aluminum, 477
Thermal stress
Plastic penetration during laser heating of a metal plate, 9
Thermo-mechanical coupling
Prediction of 3-D temperature field of TP2 copper tubes in three-roll planetary rolling process, 370
Thickness
Influence of adhesive thickness and filler content on the mechanical performance of aluminum single-lap joints bonded with aluminum powder filled epoxy adhesive, 183
Thin-wall
A parametric FEA system for fixturing of thin-walled cylindrical components, 338
Three-roll planetary rolling
Prediction of 3-D temperature field of TP2 copper tubes in three-roll planetary rolling process, 370
TiN–TiAlN
Modeling tool wear progression by using mixed effects modeling technique when end-milling AISI 4340 steel, 190
γ-Titanium aluminide
Modeling and optimization of wire electrical discharge machining of γ-TiAl in trim cutting operation, 376
Titanium
Nanocrystalline titanium produced by hydrostatic extrusion, 173
Titanium alloy
Preparation and structure of ceramic coatings containing zirconium oxide on Ti alloy by plasma electrolytic oxidation, 303
TP2 copper tube
Prediction of 3-D temperature field of TP2 copper tubes in three-roll planetary rolling process, 370
Track distance
Optimization of bead spacing during laser cladding of ZE41A-T5 magnesium alloy castings, 322
Tube bulging test
Tube bulging test: Theoretical analysis and numerical validation, 51
Turning
Investigations into the effect of cutting conditions on surface roughness in turning of free machining steel by ANN models, 16
Twist compression test
Investigation of galling in forming galvanized advanced high strength steels (AHSSs) using the twist compression test (TCT), 459
Two-dimensional cutting
Applying parallelogrammic strips for cutting circles from stainless steel rolls, 138

Upper bound
A new three-dimensional solution for the extrusions of sections with larger dimensions than the initial billet, 259
Upsetting
An analysis of formability of aluminium preforms using neural network, 272

Velocity field
A new three-dimensional solution for the extrusions of sections with larger dimensions than the initial billet, 259
Vibration endurance
Formability of tailor-welded strips and progressive forming test, 81
Viscous-elastoplasticity
A viscous-elastoplastic constitutive equation incorporating phase transformation with the application to the residual stress analysis for welding process, 316
Vision sensor
Application of circular laser vision sensor (CLVS) on welded seam tracking, 404

Water and oil repellency
Synthesis of a novel perfluorinated acrylate copolymer containing hydroxyethyl sulfone as crosslinking group and its application on cotton fabrics, 243
WC particles
Effect of WC on microstructure and mechanical properties of silicon nitride nano-composites, 411
Wear resistance
Influence of hardness on the wear resistance of 17-4 PH stainless steel evaluated by the pin-on-disc testing, 353
Wear test
Influence of hardness on the wear resistance of 17-4 PH stainless steel evaluated by the pin-on-disc testing, 353
WEDM
Modeling and optimization of wire electrical discharge machining of γ-TiAl in trim cutting operation, 376

WEDT
Statistical analysis of wire electrical discharge turning on material removal rate, 283
Welding
A viscous-elastoplastic constitutive equation incorporating phase transformation with the application to the residual stress analysis for welding process, 316
Wire tension
Application of genetic algorithm-based fuzzy logic control in wire transport system of wire-EDM machine, 128

X-ray diffraction
Microstructure and XRD analysis in the interface zone of Mg/Al diffusion bonding, 146

Zircon
Production and purification of zircon opacifier from zircon found in the coastal area of Bangladesh, 203
Zircon flour
Production and purification of zircon opacifier from zircon found in the coastal area of Bangladesh, 203
ZnO/TiO_2
Two-step solochemical synthesis of ZnO/TiO_2 nanocomposite materials, 332
ZrO_2
Preparation and structure of ceramic coatings containing zirconium oxide on Ti alloy by plasma electrolytic oxidation, 303

ELSEVIER

Volume 205, Issues 1–3, 26 August 2008

Journal of
Materials
Processing
Technology

www.elsevier.com/locate/jmatprotec

Contents

Effect of solidification rate on spatial distribution of SiC particles in A356 alloy composites 1
A. Çetin, A. Kalkanli

Plastic penetration during laser heating of a metal plate 9
Y. Chen, J. Lu, X. Ni, J. Bi, X. Zhang

Investigations into the effect of cutting conditions on surface roughness in turning of free machining steel by ANN models..... 16
J.P. Davim, V.N. Gaitonde, S.R. Karnik

Prediction of cutting forces in ball-end milling by means of geometric analysis..... 24
C.-L. Tsai, Y.-S. Liao

Relationship between subsurface damage and surface roughness of optical materials in grinding and lapping processes 34
S. Li, Z. Wang, Y. Wu

Optimization of multiple quality characteristics for CNC turning under cryogenic cutting environment using desirability function 42
A. Aggarwal, H. Singh, P. Kumar, M. Singh

Tube bulging test: Theoretical analysis and numerical validation 51
R. Velasco, N. Boudeau

Simulation of welding residual stresses in resistance spot welding, FE modeling and X-ray verification 60
I.R. Nodeh, S. Serajzadeh, A.H. Kokabi

Processing map approach for surface defect prediction in the hot bar rolling 70
H.Y. Kim, H.C. Kwon, H.W. Lee, Y.T. Im, S.M. Byon, H.D. Park

Formability of tailor-welded strips and progressive forming test..... 81
Z.Q. Sheng

Stress analysis in thin coatings and substrate subjected to point contact loading (mechanics of scratch test)..... 89
S. Rash Ahmadi, M. Shakeri, A. Sadough

A control method of guide rolls in 3D-FE simulation of ring rolling..... 99
L. Li, H. Yang, L. Guo, Z. Sun

Nanocrystalline Al–Al_2O_{3p} and SiC_p composites produced by high-energy ball milling 111
I. Ozdemir, S. Ahrens, S. Mücklich, B. Wielage

Mechanochemistry of silica on jet milling 119
S. Palaniandy, K. Azizi Mohd Azizli, H. Hussin, S. Fuad Saiyid Hashim

Application of genetic algorithm-based fuzzy logic control in wire transport system of wire-EDM machine 128
M.-T. Yan, C.-C. Fang

Applying parallelogrammic strips for cutting circles from stainless steel rolls 138
Y. Cui, X. Song

Microstructure and XRD analysis in the interface zone of Mg/Al diffusion bonding 146
J. Wang, Y. Li, P. Liu, H. Geng

(Contents continued on page I)

0924-0136(20080826)205:1/3;1-4

(Contents continued from OBC)

Consolidation of iron powders through the influence of phosphate thin films 151
J.L. Grosseau-Poussard, X. Milhet, C. Huvier, J.F. Dinhut

Crack suppression and residual stress in $BaTiO_3$ based Ni-MLCCs of Y5V specification through post-process... 160
J.-H. Kang, H.-M. Cha, Y.-G. Jung, U. Paik

Synthesis of silicon carbide/aluminium tetroxycarbide nanofibres for reinforcement of glass matrix composites: Material properties 168
P. Prapitpongwanich, K. Pengpat, P. Singjai

Nanocrystalline titanium produced by hydrostatic extrusion 173
W. Pachla, M. Kulczyk, M. Sus-Ryszkowska, A. Mazur, K.J. Kurzydlowski

Influence of adhesive thickness and filler content on the mechanical performance of aluminum single-lap joints bonded with aluminum powder filled epoxy adhesive 183
R. Kahraman, M. Sunar, B. Yilbas

Modeling tool wear progression by using mixed effects modeling technique when end-milling AISI 4340 steel 190
P. Chakraborty, S. Asfour, S. Cho, A. Onar, M. Lynn

Production and purification of zircon opacifier from zircon found in the coastal area of Bangladesh..... 203
S. Naher, A.S.M.A. Haseeb

Artificial neural network modelling of plating rate and phosphorus content in the coatings of electroless nickel plating 207
W. Yating, S. Bin, L. Lei, H. Wenbin

Fundamental studies on in-process controlling angular distortion in asymmetrical double-sided double arc welding 214
H. Zhang, G. Zhang, C. Cai, H. Gao, L. Wu

Low-pressure die casting of magnesium alloy AM50: Response to process parameters 224
P. Fu, A.A. Luo, H. Jiang, L. Peng, Y. Yu, C. Zhai, A.K. Sachdev

Theoretical and experimental investigation of mold strength in magnetic molding compacts..... 235
K.J. Suganth kumar, S. Senthilkumaran, S.R. Boopathy, A. Ramesh

Synthesis of a novel perfluorinated acrylate copolymer containing hydroxyethyl sulfone as crosslinking group and its application on cotton fabrics..... 243
Z.-R. Li, K.-J. Fu, L.-J. Wang, F. Liu

Surface finishing of hardened and tempered stainless tool steel using sequential ball grinding, ball burnishing and ball polishing processes on a machining centre..... 249
F.-J. Shiou, C.-C. Hsu

A new three-dimensional solution for the extrusions of sections with larger dimensions than the initial billet 259
K. Abrinia, M. Makaremi

An analysis of formability of aluminium preforms using neural network..... 272
G. Poshal, P. Ganesan

Statistical analysis of wire electrical discharge turning on material removal rate..... 283
A. Mohammadi, A.F. Tehrani, E. Emanian, D. Karimi

Finite-element simulation of residual stress induced by split-sleeve cold-expansion process of holes..... 290
V. Nigrelli, S. Pasta

Mixing homogeneity and its influence on the manufacturing process and properties of soft magnetic ceramics..... 297
V.T. Zaspalis, M. Kolenbrander

Preparation and structure of ceramic coatings containing zirconium oxide on Ti alloy by plasma electrolytic oxidation 303
Z. Yao, Y. Jiang, Z. Jiang, F. Wang, Z. Wu

Effect of temperature and strain rate on the compressive deformation behavior of 42CrMo steel 308
Y.C. Lin, M.-S. Chen, J. Zhong

A viscous-elastoplastic constitutive equation incorporating phase transformation with the application to the residual stress analysis for welding process 316
B. Chen, X.H. Peng, J.H. Fan, S.T. Sun

Optimization of bead spacing during laser cladding of ZE41A-T5 magnesium alloy castings 322
X. Cao, M. Jahazi, J. Fournier, M. Alain

Two-step solochemical synthesis of ZnO/TiO_2 nano-composite materials 332
M.R. Vaezi

A parametric FEA system for fixturing of thin-walled cylindrical components 338
Y. Wang, J. Xie, Z. Wang, N. Gindy

Analysis of the manufacturing process of beverage cans using aluminum alloy 347
L.F. Folle, S.E. Silveira Netto, L. Schaeffer

Influence of hardness on the wear resistance of 17-4 PH stainless steel evaluated by the pin-on-disc testing 353
J.D. Bressan, D.P. Daros, A. Sokolowski, R.A. Mesquita, C.A. Barbosa

Correlation between break-in characteristics and pad surface conditions in silicon wafer polishing 360
K. Park, H. Jeong, J. Park

Aging study of rapidly solidified and solid-solution Cu–Cr–Sn–Zn alloy 366
J.-h. Su, P. Liu, Q.-m. Dong, H.-j. Li, B.-h. Tian

Prediction of 3-D temperature field of TP2 copper tubes in three-roll planetary rolling process 370
B. Li, S.H. Zhang, G.L. Zhang, H.Q. Zhang

Modeling and optimization of wire electrical discharge machining of γ-TiAl in trim cutting operation 376
S. Sarkar, M. Sekh, S. Mitra, B. Bhattacharyya

Modeling age hardening kinetics of an Al–Mg–Si–Cu aluminum alloy 388
A.R. Eivani, A.K. Taheri

Cost and performance evaluation of different surface treated dies for hot forging process 394
M. Bayramoglu, H. Polat, N. Geren

Application of circular laser vision sensor (CLVS) on welded seam tracking 404
P. Xu, X. Tang, S. Yao

Effect of WC on microstructure and mechanical properties of silicon nitride nano-composites 411
C. Tian, N. Liu, M. Lu

Effects of light pre-deformation on pitting corrosion resistance of copper-bearing ferrite antibacterial stainless steel 419
Z.X. Zhang, G. Lin, Z. Xu

Blank design and formability prediction of complicated progressive die stamping part using a multi-step unfolding method 425
Z. Zhibing, L. Yuqi, D. Ting, L. Zhigang

$SrTi_{1-x}Zr_xO_3$ uniform particles: Low-temperature synthesis, characterization and sintered properties 432
C. Chen, Y. Wei, D. Chen, X. Jiao

Study on prediction of surface quality in machining process 439
C. Lu

Analysis and design of body jack case stamping for fewer production steps 451
T. Buranathiti, A. Kositpipat

Investigation of galling in forming galvanized advanced high strength steels (AHSSs) using the twist compression test (TCT) 459
H. Kim, J. Sung, F.E. Goodwin, T. Altan

Stress analysis of rectangular cup drawing 469
D. E, T. Mizuno, Z. Li

Microstructure, temperature estimation and thermal shock resistance of PEO ceramic coatings on aluminum 477
D.-J. Shen, Y.-L. Wang, P. Nash, G.-Z. Xing

Optimization of superplastic hydroforming process of Aluminium alloy 5083 482
M.H. Hojjati, M. Zoorabadi, S.J. Hosseinipour

Microwave assisted sintering of green metal parts 489
C. Leonelli, P. Veronesi, L. Denti, A. Gatto, L. Iuliano

Analysis of metal workability by integration of FEM and 3-D processing maps 497
J. Liu, Z. Cui, C. Li

Modeling of hot tearing formation during solidification 506
N. Hatami, R. Babaei, M. Dadashzadeh, P. Davami

Author index 514

Subject index 516